

Nanoplasmonic colloidal suspensions for the enhancement of the luminescent emission from single-walled carbon nanotubes

Mareen Glaeske and Antonio Setaro (✉)

Department of Physics, Freie Universität Berlin, Arnimallee 14, 14195 Berlin, Germany

Received: 30 January 2013

Revised: 18 May 2013

Accepted: 19 May 2013

© Tsinghua University Press
and Springer-Verlag Berlin
Heidelberg 2013

KEYWORDS

carbon nanotubes,
luminescence enhancement,
gold nanorods,
nanoplasmonic colloids,
hybrid structures

ABSTRACT

Aiming to enhance the luminescence yield of carbon nanotubes, we introduce a new class of hybrid nanoplasmonic colloidal systems (π -hybrids). Nanotubes dispersed in gold nanorod colloidal suspensions yield hybrid structures exhibiting enhanced luminescence up to a factor of 20. The novelty of the proposed enhancement mechanism relies on including metal proximity effects in addition to its localized surface plasmons. This simple, robust and flexible technique enhances the luminescence of nanotubes with chiralities whose enhancement has never reported before, for example the (8,4) tube.

1 Introduction

In the world at nano scale, carbon nanotubes (CNTs) stand out for their exceptional mechanical, optical, and electronic properties [1]. Single walled carbon nanotubes (SWNTs) can be seen as a graphene sheet cut and rolled up along a certain direction, described by the so-called chiral vector $c = \{n_1, n_2\}$. The boundary conditions resulting from this process introduce quantization of the tube's allowed electronic states. As a consequence, there are both nanotubes with metallic character and nanotubes with a band-gap.

In semiconducting nanotubes, luminescence can be observed. The photon energies involved in the process uniquely identify a tube with a given chirality [2, 3]. The photo-generated electrons and holes form strongly bound excitons with binding energies from few tens of meV up to 1 eV, which dominate the optical spectra of SWNTs [4, 5]. The photoluminescence (PL) yield of SWNTs is very low-typically around 3% for single suspended nanotubes, or 0.05% for nanotube solutions [6–8]. The highest yield reported so far is 20% for CNTs dispersed with special oxygen-excluding surfactants [9]. Several routes have been pursued to overcome

Address correspondence to setaro@physik.fu-berlin.de.

this limit and enhance the luminescence of the tubes, for example through energy transfer between dye molecules and SWNTs [10], by including tubes into optical cavities made with metallic [11] or dielectric [12] mirrors, and by exploiting photonic crystals [13]. The luminescence enhancement achieved in all these experiments is driven by the same physical two mechanisms, namely either stronger pumping of the excited state or speeding up the radiative de-excitation rate. The metal-induced PL enhancement seems to be particularly promising, because, engineering the experimental parameters, both mechanisms contribute to the luminescence enhancement. Metal-induced enhancement was shown to enhance PL signals for molecular fluorophores. It is based on the fact that the proximity of the metal surface will cause additional de-excitation rate [14]. Under the proper conditions [15], this additional de-excitation rate due to the metal presence will cause a shortening of the decay times as well as an enhancement of the PL quantum yield. Additionally, the quantum yield can be further affected by exploiting structured metal surfaces, where the electric fields get strongly enhanced through bright localized surface plasmons (LSPs). The surface morphology, the plasmon wavelength λ_{π} and the electric field enhancement are the key parameters in such systems. Adapting the expression in Ref. [16], the emission quantum yield, given by the PL enhancement factor, can be written as

$$Q_{m,\pi} = I_m / I_0 = \eta(\lambda_{\pi}, d) Q_m(d) \quad (1)$$

where $Q_m(d) = (\gamma_R + \gamma_{NR}) / (\gamma_R + \gamma_{NR} + \gamma_m(d))$ accounts for the proximity effects and γ_s is the decay rates (respectively, γ_R is radiative, γ_{NR} non-radiative, and γ_m due to the exciton transfer from the molecule to the metal surface). $\eta(\lambda_{\pi}, d) = |E(\lambda_{\pi}, d)/E_0|^2$ is the electric field enhancement observed in case the wavelength of the exciting laser matches the plasmonic features of the metallic system. Thus the nanostructuring of the metal surfaces will give an extra contribution to the metal-enhancement of the optical properties of a fluorophore. Please note that LSPs require a certain tube-metal separation (cf. Ref. [16]) in order to induce PL enhancement. For this reason we will refer in the rest of the paper to plasmonic enhancement as to the contribution to the LSPs while we will refer as proximity effects for the other mechanisms. It is worth

noting the neat effect of the two terms in Eq. (1), as they will be easily distinguished in a photoluminescence excitation (PLE) chart: While Q_m depends upon both metal and fluorophore, η depends only upon the metal. The intensity-enhanced localized surface plasmons, which lead to a stronger pumping of the fluorophore, possess a specific wavelength λ_{π} . Hence only pumping the system at this specific wavelength the enhanced pumping mechanism occurs: The effect will thus appear along the horizontal direction in a PLE chart (i.e., at a fixed excitation wavelength). The term Q_m containing the proximity effects is observable everywhere in the chart, not being limited to certain excitation wavelengths.

Various nanostructured metal systems have been synthesized. An inspiring review on this topic can be found in Ref. [17]. The value of the field enhancement and the coupling with the fluorophores depend upon the morphology of the nanostructured material; the details remain an open theoretical and computational challenge.

The presence of metallic nanoparticles was exploited to enhance the optical properties of more elaborate structures than simple molecular fluorophores. For example it was proven that the enhanced electromagnetic field in between two gold nanodisks dimer lead to enhanced Raman features of graphene [18]. Furthermore, a three-fold enhancement of the (7,5) SWNT PL emission intensity was observed on a sputtered Au surface [16], whereas a ten-fold enhancement of tubes with E_{22} transition energies around 650 nm ((7,5), (7,6), and (10,3)), was reported for a highly porous surface directly grown from Au nanoparticles [19]. In both studies, the PL was enhanced for nanotubes of specific chiralities, whose electronic properties matched the frequency window of the surface plasmons. These chiralities all lie along a single excitation line, i.e., 650 nm, in a PLE chart. The physical mechanism behind the enhancement is rooted in the $\eta(\lambda_{\pi}, d)$ term in Eq. (1).

The key idea of the present work lies in the growth of gold nanoparticles with tailored features.

Our approach is doubly advantageous: by rationally synthesizing the gold nanostructure with specific plasmonic features, we address carbon nanotubes of targeted chiralities, accessing also those tubes outside

the resonance window of the previous experimental reports. Moreover, by tuning the aspect ratio and shape of the nanoparticle, we realize structures with improved electric field enhancement. In this way we take advantage of both terms in Eq. (1) for achieving optimal enhancement. Another peculiarity of our approach lies in the fact that, instead of casting the gold nanostructures on a surface, we keep them in aqueous solution, realizing a nanoplasmonic colloidal suspension.

Nanoplasmonic colloids were successfully exploited to enhance the fluorescence of several systems, in particular in systems of biological interest, where working in a water suspension is fundamental [20]. CNTs have been profitably included in biological systems [21–23]. Including luminescence-enhanced SWNTs in nanoplasmonic colloidal dispersions and creating hybrid plasmonic (π -hybrids) colloids would help implementing suspensions with bright markers emitting in the near-infrared window of biological tissues. Please note that the π of our π -hybrids has been chosen to highlight their plasmonic character and does not refer to the nature of the chemical bond holding the constituents together. A last advantage of the proposed system is its robustness and flexibility: While other enhancement methods do work in special configurations realized for the fundamental investigations but cannot be integrated in real systems without loss of the enhancement, the colloidal suspensions can be profitably integrated without loss, for example, in biological systems [19].

2 Experiments and discussion

We worked with gold nanorods (AuNR) for sake of simplicity of preparation and characterization. For details on the synthesis and characterization of the colloidal suspension made by suspending AuNR with CTAB in water, please see the Electronic Supplementary Material (ESM). We will refer to the AuNR suspension for the rest of this paper as the mother solution. A TEM picture of the AuNR synthesized for this work can be found in Fig. 1. The resulting AuNRs had an average length of 100 nm and average width of 20 nm (see Fig. 1) and the resonance wavelength of the longitudinal (LP) and transverse plasmons (TP) were, respectively,

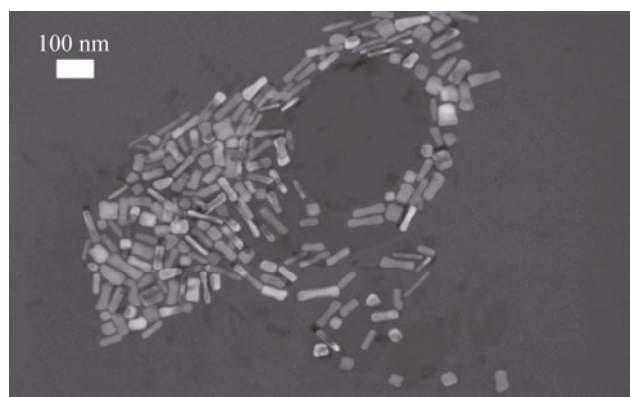


Figure 1 TEM picture of the AuNR synthesized for this work. The rod particles are 100 nm long and 20 nm width on the average.

740 nm and 520 nm, as it can be seen in Fig. 2(a). The nanotube solubilization was performed following the stirring method in CTAB reported in Ref. [24] and an adapted version of the stirring method was exploited in order to promote the π -hybrid formation. Details on the experimental procedure can be found in the Electronic Supplementary Information (ESI). It is worth noting that this is the only method promoting the hybrid formation; sonication, for example, does not yield any hybrids. Basically, our hybridization process can be seen as an adapted version of the micelle swelling technique [25]: In a water suspension of micelle-stabilized nano-objects (in our case, the

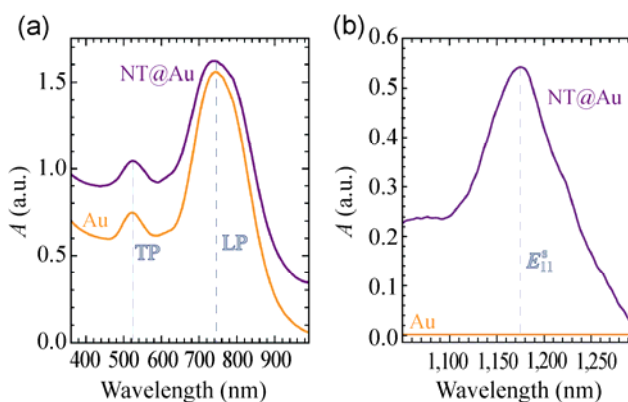


Figure 2 (a) Absorption spectra of the AuNR suspension (orange curve labeled as Au) and of the SWNT-AuNRs complexes (purple curve labeled as NT@Au). The two absorption bands called TP and LP correspond to the transversal and longitudinal plasmon frequencies. (b) IR Absorption spectra of the AuNR suspension (orange curve labeled as Au) and of the SWNT@Au complexes (purple curve labeled as NT@Au). In this region, the gold does not absorb and only the E_{11}^S nanotube absorption band can be observed.

CTAB-stabilized AuNRs) we add some additional, non-water soluble objects (in our case, the SWNTs). As the tubes are not soluble in water, they can either (a) precipitate or (b) be encapsulated within the gold-containing micelles. The micelle filling process has to be performed by following the gentle stirring procedure, otherwise the AuNR-containing micelle get broken, the equilibrium and composition of the object suspended in the samples get altered and Au precipitation can be observed. This is the reason why the sonication method cannot lead to any hybrid formation in our case. This process of encapsulation of the tubes within the micelles can go on up to a certain limit of the micelle loading. There is thus a certain amount of tubes to add to the starting solution beyond which no further encapsulation is possible and the excess of tubes will start precipitating. In the following, we will refer to the π -hybrid colloidal dispersion as NT@Au. Please note that the visible part of the absorption spectrum of the

NT@Au suspension is dominated by the plasmonic features of the gold nanorods (Fig. 2(a)). In the NIR part of the spectrum, on the contrary, the E_{11}^S transition bands of the semiconducting SWNTs are the predominant feature (Fig. 2(b)). As no contribution from Au absorption occurs in this range, the E_{11}^S band can be usefully exploited as indicator of the total amount of tubes encapsulated within the π -hybrids.

As the metal-fluorophore distance plays an important role in the metal-enhancement of the luminescence, we decided to change the nanotube density in the solution in order to try and affect the tubes-to-rods relative ratio. In Fig. 3(b) the PL intensity of the (7,5) and (7,6) tubes is shown for different amounts of tubes added to the mother solution. In the following, we will refer to the SWNTs stirred in the mother solution as NT@Au. In a typical suspension of SWNTs sonicated in CTAB the intensity of the (7,5) peak is 1.5 times stronger than the (7,6) one. As visible in Fig. 3(b), in the

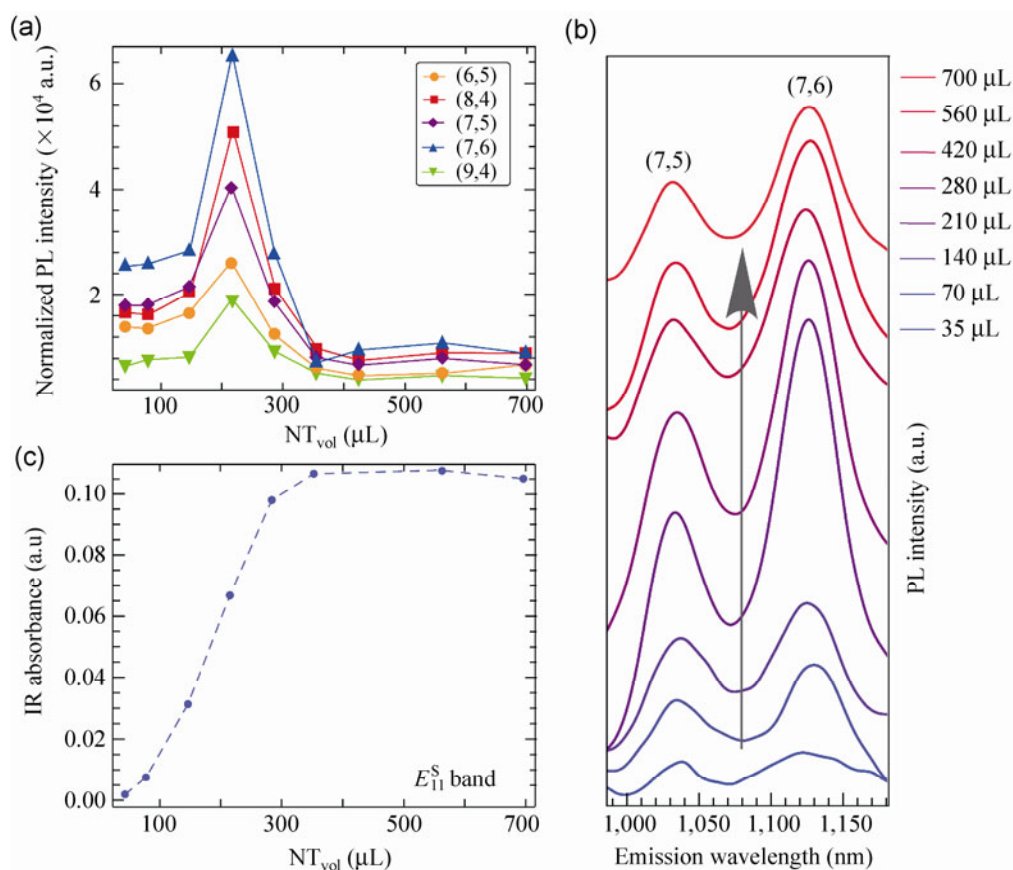


Figure 3 (a) Normalized intensity of the PL emission of tubes with different chiralities for different amount of SWNTs added to the mother solution. The spectra have been normalized by the density of tubes in the final suspensions. (b) PL emission of the (7,5) and (7,6) tubes for different starting SWNTs concentration. The traces are offset for clarity. (c) Intensity of the E_{11}^S absorption band at 1,175 nm as an estimation of the amount of tubes present in the final suspensions.

NT@Au samples the intensity ratio between the two emission bands is inverted, which is already a first indication that the interaction with the AuNRs is actually affecting the tubes. The inversion of the intensity of the (7,5) and (7,6) tubes is accompanied by a nonmonotonous change of the peak intensities when tuning the nanotube-to-nanorod ratio. When increasing the fraction, PL emission increases up to a certain level before it starts to decrease again. In Fig. 3(a) the intensities of the PL for all the tubes present in solution are reported; the spectra have been normalized by the density of tubes in the final suspensions for estimating of the average emission per tube. The original uncorrected intensities as well as the IR absorption spectra can be found in Fig. S1 in the ESM. A similar behaviour, with the intensity reaching a maximum and then decreasing, is shared by all chiralities. To rule out that the lowering of the PL intensity results from a loss of material, we compare the PL intensity with the intensity of the E_{11}^S absorption band in Fig. 3(c). The absorption can be taken as an indicator of the amount of the tubes present in solution [24]. Starting from 210 μL and adding bigger amount of tubes, we observe that the overall luminescence of the tubes decreases (cf. Fig. 3(a)) while the amount of tubes in suspension keeps increasing. We assume that in this region the number of SWNTs within the micelles starts becoming high enough to make tube–tube interaction and related quenching phenomena relevant. Starting from amount of tubes bigger than 400 μL , we assume that we reach the maximum load of the micelles; this is supported by the observation of precipitate formation in our samples, given by the excess of tubes. This accounts also for the observed saturated trend of the absorption spectra (Fig. 3(c)): The density of tubes in the final suspension remains constant, even by starting with higher amount of tubes.

So far we have only reported on the behaviour of the luminescence of the NT@Au; in order to estimate the enhancement of the PL, we compared our best NT@Au samples (the one showing the highest PL intensity, corresponding to 210 μL NT_{VOL}) with a sample prepared by following exactly the same procedure but using a solution with only CTAB (without any AuNR) instead of the mother solution. We will refer to such a sample in the rest of the paper as

NT@CTAB. Figure 4 shows the histogram distribution of the intensities of the PL emissions for the different tubes present in our samples. The distribution of the intensities between the various chiralities is altered after the interaction with the AuNRs. The most striking effect, however, is the strong enhancement of the PL emission when the tubes interact with the gold nanoparticles. In the inset of Fig. 4 the histogram distribution of the ratio between the intensities of NT@Au and NT@CTAB is reported. We enhance the PL intensity of the tube chirality (8,4) by a factor of 20. The (7,6) tube luminescence gets enhanced by a factor of eight, which is a value comparable with the one reported for NT deposited on a porous Au surface [19]. The correlation between enhancement, tube chirality and metallic particle plasmonic features will be object of future investigations. This experiment is a proof of concept for the PL enhancement in π -hybrids colloidal suspensions. The authors believe that there is still a large margin of improvement by optimizing the amount of AuNR in the mother solution, the morphology of the nanoparticles, as well as the choice of metal.

In order to further confirm the efficiency of the proposed PL enhancing system, we compared our NT@Au sample with SWNTs in a CTAB suspension prepared following the standard preparation (i.e., sonication and centrifugation). For the description of the standard preparation procedure of such a

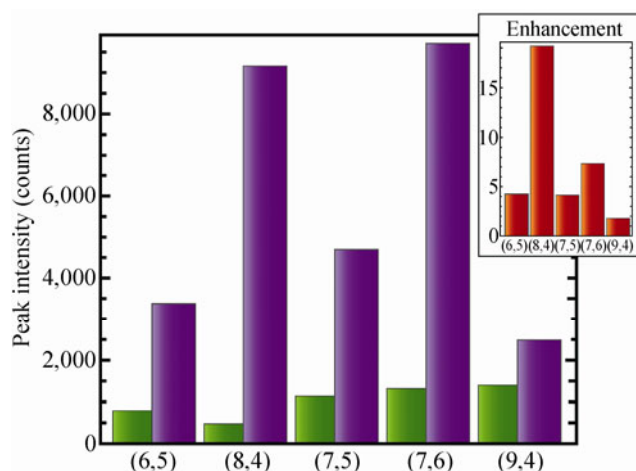


Figure 4 Histogram of the distribution of the PL intensities of the NT@Au (purple) and for the NT@CTAB (green) samples. The inset reports the histogram of the distribution of the enhancement of NT@Au intensity with respect to the NT@CTAB sample.

suspension, please refer to any of our past works [26, 27]. We will refer in the text and in the figures to such a sample just as CTAB. The comparison between the NT@Au and the CTAB sample in Fig. 5 highlights the benefits of our systems: By moving along the α excitation lines of the PLE charts (cf. Fig. 5(c)) one can observe a very pronounced enhancement of the fluorescent emission of the (7,6) and the (8,4) chiralities. Surprisingly, no enhancement for the (9,4) tube can be observed. Similarly, by moving along the β emission lines (Fig. 5(d)), the intensity of the (7,5) tube is approximately the same in both samples while the (7,6) gets enhanced. This behavior highlights the originality of our system: The enhancement occurs in several regions of the PLE chart, revealing that the π -hybrids take advantage of proximity effects (the Q_m term in Eq. (1)), unlike previous works [16, 19] that only resorted to localized surface plasmons (the η term in

Eq. (1)) and was limited to the 650 nm excitation line. It is worth pointing out that the spectral position of the PLE peaks in addition to their relative intensities are altered by the presence of AuNRs. Surprisingly, the emission wavelength is strongly affected while the excitation is not. This rules out the solvatochromic shift [28] (which would affect in a similar fashion both excitation and emission wavelengths), or electric dipole-nanotube interaction [29–32]. Indeed, this behaviour has been observed and modelled for an analogous system constituted by a low-quantum yield nanostructured semiconductor (CdTe nanowires) interacting with gold nanoparticles [33]. At an optimal semiconductor-metal distance, the sample exhibited the same phenomenology as our samples. This has been proven [33] to be consequence of the excitons-plasmon interaction in the hybrid superstructure: At an optimal metal-semiconductor distance, a significant

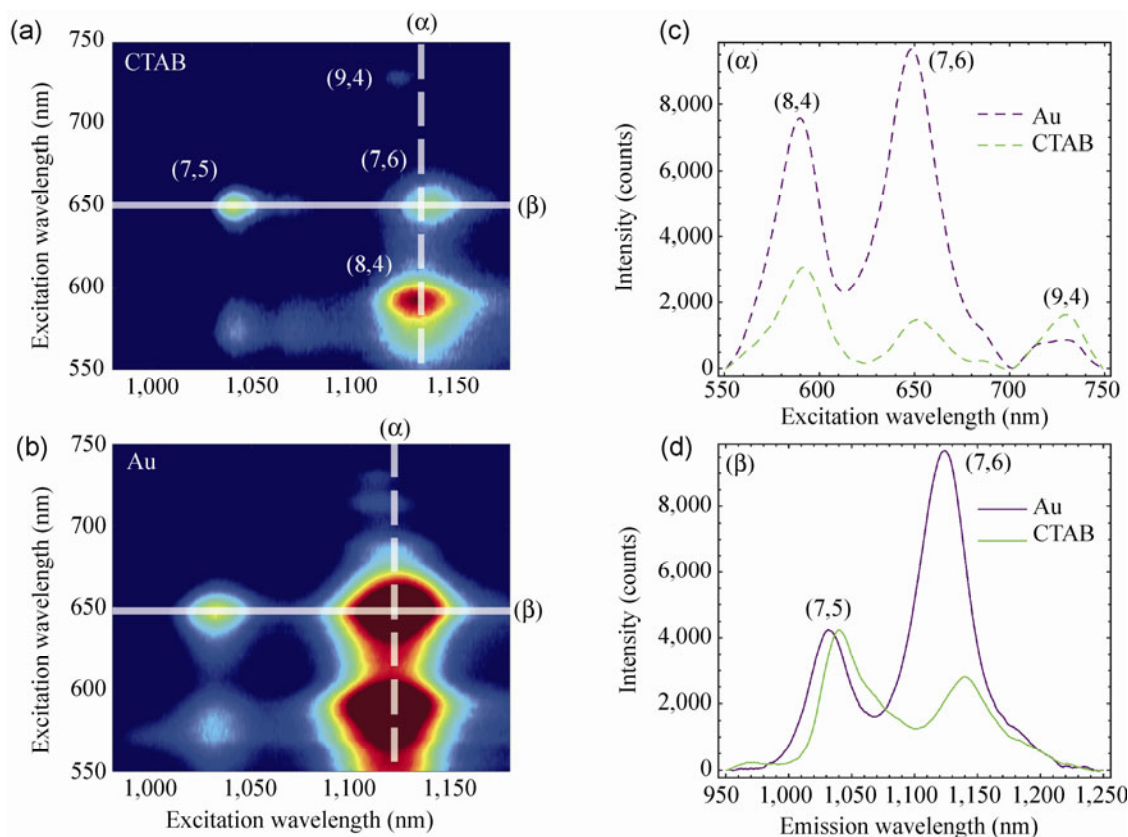


Figure 5 (a) PLE chart of the CTAB sonicated sample. (b) PLE chart of the NT@Au sample. The dotted lines denoted with an α represent a single excitation line taken in at the maximum of the (7,6), (8,4) emission intensities, while the continuous lines denoted with a β are single emission lines taken at the excitation maximum of the (7,5), (7,6) tubes. Please note that the emission wavelength of the NT@Au sample differ from the one of the CTAB sample, indicating an interaction with the AuNRs. (c) Comparison of the single excitation lines of the NT@Au sample with the CTAB sample. (d) Comparison of the single emission lines of the NT@Au sample with the CTAB sample.

shortening of the excitonic lifetimes occurs with consequent blue shift of the emitted spectra. The presence of the blue shift in the spectra emitted by our π -hybrids can be depicted in the framework of the results of Ref. [33] as consequence of the nanotube-exciton metal-plasmon coupling. Please note that no overlap between gold plasmonic features and nanowires energy bands are present in the experiment of Ref. [33]; we assume that this is the reason why no enhancement of the luminescence has been observed there.

In order to investigate the relation of the emission enhancement and blue shifts vs. interaction strengths between the constituents of the π -hybrids, several sonication steps were applied to the stirred samples NT@Au and NT@CTAB. Sonication is a high-energetic treatment that does not lead to any hybrid formation and any metal-induced PL enhancement (see the ESM) and is thus expected to promote further isolation of tubes from small bundles and to possibly break some π -hybrids into their original constituents. For this reason, sonication can be used as a tool for testing the strength of the interaction yielding the π -hybrids. The emission bands of the (7,5) and (7,6) chiralities have been monitored during the process and are reported in Fig. 6. The solutions were exposed to short sonication periods of, respectively, 2, 4, and 14 min. Noticeably, this simple experiment reveals different trends for the (7,5) and the (7,6) tubes: The emitted intensity of the (7,5) tube behaves in a similar manner in both samples

with and without gold, increasing with increasing sonication times. The intensity of the (7,6) tube, on the contrary, behaves differently in the Au@NT and CTAB samples: In the gold solution its intensity remains the same, unaffected by the sonication steps (cf. Fig. 6(a)). Also the spectral position of the bands reveals different trends: after just the first sonication step, the spectral position of the (7,5) tube in the NT@Au suspension reaches the position of the free (7,5) tube and no blue shift can be observed through the other sonication steps (cfr. Figs. 6(b) and (c)). For the (7,6) tube, on the contrary, the spectral position of the sample still evolves under the different sonication steps (cf. Fig. 6(b)) but the blue shift between the emission of the tube in the NT@Au and the NT@CTAB solutions persists and is not destroyed by the sonication treatment (cf. Fig. 6(c)). This different response suggests that the (7,5)@Au complex is weakly bound and can easily get broken while the (7,6)@Au π -hybrid is strongly bound, does not get set apart and remains unperturbed even after sonication. It is worth pointing out that binding strength and PL enhancement are strictly related in our samples.

In order to draw any general conclusion, anyway, analysis of samples with a broader set of chiralities needs to be carried out. The systematic correlation between PL enhancement, blue shifts, stability of the complexes and the selective chemistry behind these phenomena will be object of future investigations.

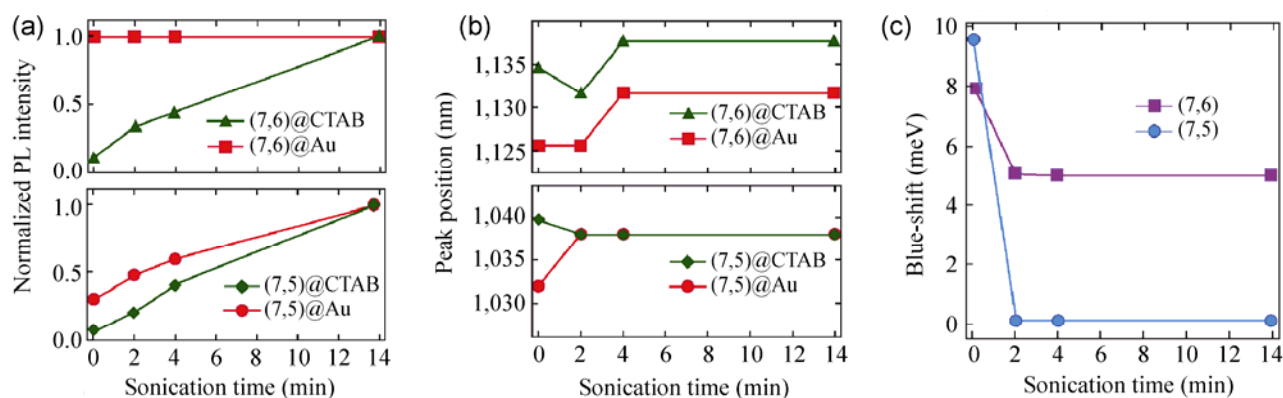


Figure 6 (a) Intensity of the PL emission bands of the (7,5) and (7,6) tubes (normalized by setting to 1 the intensity after the last sonication step) of the NT@Au and NT@CTAB samples after different sonication steps (0, 2, 4, and 14 min, respectively), (b) Spectral position of the PL emission bands of the (7,5) and (7,6) tubes of the NT@Au and NT@CTAB samples after the different sonication steps, and (c) Au-induced blue shifts of the emission bands of the (7,5) and (7,6) tubes after the different sonication steps.

3 Conclusions

In conclusion, by exploiting a nanoplasmonic colloidal suspension of gold nanorods, we have implemented π -hybrid (gold nanorod-carbon nanotubes hybrid structures) colloidal suspensions which exhibit a 20-fold enhanced photoemission with respect to isolated single walled carbon nanotubes. The physical mechanisms behind the achieved enhancement can be ascribed to more complex phenomena than the previously reported mechanisms: Not only surface localized electric fields but also proximity effects do contribute to the overall enhancement effect. Altering the morphology of the nanoplasmonic particle may result in an even higher contribution to the luminescence enhancement due to the stronger localized electric fields [34]. Working in suspension offers the advantage of easing experimental access to the fundamental optical properties of the π -hybrids. Moreover, this approach yields strongly IR-luminescent suspensions that can profitably be integrated in biological systems. The potential of this technique lies in its simplicity, robustness, and flexibility, as a huge variety of metal nanostructured particles can be easily synthesized with plasmonic and morphological features tailored to match nanotubes with targeted chiralities. We have proven this principle in the enhancement of the luminescence of the (8,4) tube, whose luminescence enhancement has never been reported before in literature.

Acknowledgements

The authors gratefully thank the FU Focus Area NanoScale for financial support; parts of the work were supported by the DFG under the SFBI 658. The authors thank P. Bluemmel, F. Ernst, and S. Heeg for useful discussions and S. Reich for a critical reading of the manuscript.

Electronic Supplementary Material: Supplementary material describing the experimental procedure for the gold nanorod synthesis, the hybridization route as well as the characterization procedure is available in the online version of this article at <http://dx.doi.org/10.1007/s12274-013-0335-5>.

References

- [1] Reich, S.; Thomsen, C.; Maultzsch, J. *Carbon Nanotubes: Basic Concepts and Physical Properties*; Wiley-VCH: Berlin, 2004.
- [2] O'Connell, M. J.; Bachilo, S. M.; Huffman, C. B.; Rialon, K. L.; Boul, P. J.; Noon, W. H. Band gap fluorescence from individual single-walled carbon nanotubes. *Science* **2002**, *297*, 593–596.
- [3] Bachilo, S. M.; Strano, M. S.; Kittrell, C.; Hauge, R. H.; Smalley, R. E.; Weisman, R. B. Structure-assigned optical spectra of single-walled carbon nanotubes. *Science* **2002**, *298*, 2361–2366.
- [4] Maultzsch, J.; Pomraenke, R.; Reich, S.; Chang, E.; Prezzi, D.; Ruini, A.; Molinari, E.; Strano, M. S.; Thomsen, C.; Lienau, C. Exciton binding energies in carbon nanotubes from two-photon photoluminescence. *Phys. Rev. B* **2005**, *72*, 241402.
- [5] Wang, F.; Dukovic, G.; Brus, L. E.; Heinz, T. F. The optical resonances in carbon nanotubes arise from excitons. *Science* **2005**, *308*, 838–841.
- [6] Ernst, F.; Heek, T.; Setaro, A.; Haag, R.; Reich, S. Energy transfer in nanotube-perylene complexes. *Adv. Funct. Mater.* **2012**, *22*, 3921–3926.
- [7] Carlson, L. J.; Maccagnano, S. E.; Zheng, M.; Silcox, J.; Krauss, T. D. Fluorescence efficiency of individual carbon nanotubes. *Nano Lett.* **2007**, *7*, 3698–3703.
- [8] Jones, M.; Engtrakul, C.; Metzger, W. K.; Ellingson, R. J.; Nozik, A. J.; Heben, M. J.; Rumbles, G. Analysis of photoluminescence from solubilized single-walled carbon nanotubes. *Phys. Rev. B* **2005**, *71*, 115426.
- [9] Ju, S.; Kopcha, W.; Papadimitrakopoulos, F. Brightly fluorescent single-walled carbon nanotubes via an oxygen-excluding surfactant organization. *Science* **2009**, *323*, 1319–1323.
- [10] Ahmad, A.; Kern, K.; Balasubramanian, K. Selective enhancement of carbon nanotube photoluminescence by resonant energy transfer. *ChemPhysChem* **2009**, *10*, 905–909.
- [11] Xia, F.; Steiner, M.; Lin, Y. M.; Avouris, P. A microcavity-controlled, current-driven, on-chip nanotube emitter at infrared wavelengths. *Nat. Nanotechnol.* **2008**, *3*, 609–613.
- [12] Gauffrès, E.; Izard, N.; Roux, X. L.; Kazaoui, S.; Marris-Morini, D.; Cassan, E.; Vivien, L. Optical microcavity with semiconducting single-wall carbon nanotubes. *Opt. Express* **2010**, *18*, 5740–5745.
- [13] Watahiki, R.; Shimada, T.; Zhao, P.; Chiashi, S.; Iwamoto, S.; Arakawa, Y.; Maruyama, S.; Kato, Y. K. Enhancement of carbon nanotube photoluminescence by photonic crystal nanocavities. *Appl. Phys. Lett.* **2012**, *101*, 141124.

- [14] Lakowicz, J. R.; Shen, Y.; D'Auria, S.; Malicka, J.; Fang, J.; Gryczynski, Z.; Gryczynski, I. Radiative decay engineering: 2. Effects of silver island films on fluorescence intensity, lifetimes, and resonance energy transfer. *Anal. Biochem.* **2002**, *301*, 261–277.
- [15] Ming, T.; Chen, H.; Jiang, R.; Li, Q.; Wang, J. Plasmon-controlled fluorescence: Beyond the intensity enhancement. *J. Phys. Chem. Lett.* **2012**, *3*, 191–202.
- [16] Sakashita, T.; Miyauchi, Y.; Matsuda, K.; Kanemitsu, Y. Plasmon-assisted photoluminescence enhancement of single-walled carbon nanotubes on metal surfaces. *Appl. Phys. Lett.* **2010**, *97*, 063110.
- [17] Halas, N. J. Plasmonics: An emerging field fostered by nano letters. *Nano Lett.* **2010**, *10*, 3816–3822.
- [18] Heeg, S.; Fernandez-Garcia, R.; Oikonomou, A.; Schedin, F.; Narula, R.; Maier, S. A.; Vijayaraghavan, A.; Reich, S. Polarized plasmonic enhanced by au nanostructures probed through Raman scattering of suspended grapheme. *Nano Lett.* **2013**, *13*, 301–308.
- [19] Hong, G.; Tabakman, S. M.; Welsher, K.; Wang, H.; Wang, X.; Dai, H.; Matsuda, K.; Kanemitsu, Y.; Irie, K.; Saiki, T.; Someya, T.; Miyauchi, Y.; Maruyama, S. Metal-enhanced fluorescence of carbon nanotubes. *J. Am. Chem. Soc.* **2010**, *132*, 15920–15923.
- [20] Deng, W.; Goldys, E. M. Plasmonic approach to enhanced fluorescence for applications in biotechnology and the life sciences. *Langmuir* **2012**, *28*, 10152–10163.
- [21] Cherukuri, P.; Bachilo, S. M.; Litovsky, S. H.; Weisman, R. B. Near-infrared fluorescence microscopy of single-walled carbon nanotubes in phagocytic cells. *J. Am. Chem. Soc.* **2004**, *126*, 15638–15639.
- [22] Leeuw, T. K.; Reith, R. M.; Simonette, R. A.; Harden, M. E.; Cherukuri, P.; Tsybouski, D. A.; Beckingham, K. M.; Weisman, R. B. Single-walled carbon nanotubes in the intact organism: Near-IR imaging and biocompatibility studies in drosophila. *Nano Lett.* **2007**, *7*, 2650–2654.
- [23] Welsher, K.; Liu, Z.; Sherlock, S. P.; Robinson, J. T.; Chen, Z.; Daranciang, D.; Dai, H. A route to brightly fluorescent carbon nanotubes for near-infrared imaging in mice. *Nat. Nanotechnol.* **2009**, *4*, 773–780.
- [24] Wenseleers, W.; Vlasov, I.; Goovaerts, E.; Obratsova, E.; Lobach, A.; Bouwen, A. Efficient isolation and solubilization of pristine single-walled nanotubes in bile salt micelles. *Adv. Funct. Mater.* **2004**, *14*, 1105–1112.
- [25] Wang, R. K.; Chen, W. C.; Campos, D. K.; Ziegler, K. J. Swelling the micelle core surrounding single-walled carbon nanotubes with water-immiscible organic solvents. *J. Am. Chem. Soc.* **2008**, *130*, 16330–16337.
- [26] Setaro, A.; Popeney, C. S.; Trappmann, B.; Datsyuk, V.; Haag, R.; Reich, S. Polyglycerol-derived amphiphiles for single walled carbon nanotube suspension. *Chem. Phys. Lett.* **2010**, *493*, 147–150.
- [27] Popeney, C. S.; Setaro, A.; Mutihac, R. C.; Bluemmel, P.; Trappmann, B.; Vonneman, J.; Reich, S.; Haag, R. Polyglycerol-derived amphiphiles for the solubilization of single-walled carbon nanotubes in water: A Structure-property study. *ChemPhysChem* **2012**, *13*, 203–211.
- [28] Choi, J. H.; Strano, M. S. Solvatochromism in single-walled carbon nanotubes. *Appl. Phys. Lett.* **2007**, *90*, 223114.
- [29] Malic, E.; Weber, C.; Richter, M.; Atalla, V.; Klamroth, T.; Saalfrank, P.; Reich, S.; Knorr, A. Microscopic model of the optical absorption of carbon nanotubes functionalized with molecular spiropyran photoswitches. *Phys. Rev. Lett.* **2011**, *106*, 097401.
- [30] Setaro, A.; Bluemmel, P.; Maity, C.; Hecht, S.; Reich, S. Non-covalent functionalization of individual nanotubes with spiropyran-based molecular switches. *Adv. Funct. Mater.* **2012**, *22*, 2425–2431.
- [31] Bluemmel, P.; Setaro, A.; Maity, C.; Hecht, S.; Reich, S. Tuning the interaction between carbon nanotubes and dipole switches: The influence of the change of the nanotube–spiropyran distance. *J. Phys.: Condens. Mat.* **2012**, *24*, 394005.
- [32] Cambré, S.; Santos, S. M.; Wenseleers, W.; Nugraha, A. R. T.; Saito, R.; Cognet, L.; Lounis, B. Luminescence properties of individual empty and water-filled single-walled carbon nanotubes. *ACS Nano* **2012**, *6*, 2649–2655.
- [33] Lee, J.; Hernandez, P.; Lee, J.; Govorov, A. O.; Kotov, N. A. Exciton-plasmon interactions in molecular spring assemblies of nanowires and wavelength-based protein detection. *Nat. Mater.* **2007**, *6*, 291–295.
- [34] Kou, X.; Ni, W.; Tsung, C. K.; Chan, K.; Lin, H. Q.; Stucky, G.; Wang, J. Growth of gold bipyramids with improved yield and their curvature-directed oxidation. *Small* **2007**, *3*, 2103–2013.